JACS
JOURNAL OF THE AMERICAN CHEMICAL SOCIETY
Article
pubs.acs.org/JACS

Mobility Mechanism of Hydroxyl Radicals in Aqueous Solution via Hydrogen Transfer

Edelsys Codorniu-Hernández and Peter G. Kusalik*

Department of Chemistry, University of Calgary, 2500 University Drive NW, Calgary T2N1N4, Alberta, Canada

Supporting Information

ABSTRACT: The hydroxyl radical (OH*) is a highly reactive oxygen species that plays a salient role in aqueous solution. The influence of water molecules upon the mobility and reactivity of the OH* constitutes a crucial knowledge gap in our current understanding of many critical reactions that impact a broad range of scientific fields. Specifically, the relevant molecular mechanisms associated with OH* mobility and the possibility of diffusion in water via a H-transfer reaction remain open questions. Here we report insights into the local hydration and electronic structure of the OH* in aqueous solution from Car−Parrinello molecular dynamics and explore the mechanism of H-transfer between OH* and a water molecule. The relatively small free energy barrier observed (~4 kcal/mol) supports a conjecture that the H-transfer can be a very rapid process in water, in accord with very recent experimental results, and that this reaction can contribute significantly to OH* mobility in aqueous solution. Our findings reveal a novel H-transfer mechanism of hydrated OH*, resembling that of hydrated OH^- and presenting hybrid characteristics of hydrogen-atom and electron−proton transfer processes, where local structural fluctuations play a pivotal role.

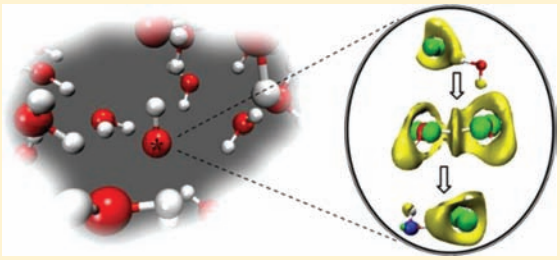

INTRODUCTION

The hydroxyl radical (OH*) is a highly reactive species that is ubiquitous in our environment. It plays crucial roles in diverse fields ranging from water remediation and environmental cleanup, radiation processing and nuclear reactors, to medical diagnosis and therapy.[1] OH* is a critical chemical species in the lower atmosphere,[2,3] it is an essential compound to the body's natural defense mechanisms,[4] and is believed to be responsible for damage to DNA, lipids, and proteins. Yet, its reactivity is apparently strongly influenced by water molecules.[5,6] The possible existence of a H_2O−OH* complex has been speculated to affect strongly the diffusion and oxidative capacity of the radical. Particularly, the [H_2O--HO*] interaction in which OH* acts as a H-bond donor has been found as a minimum in the potential energy surface of OH*−H_2O dimers in the gas phase.[7−11] However, direct experimental measurements of transient neutral species is very challenging, and indeed the data available for OH* are limited.[1] The temperature dependence of the OH* diffusion coefficient, for example, has only been estimated by assuming Stokes law behavior or by assuming the temperature dependence is the same as for water self-diffusion.[1]

In addition to a molecular mechanism, OH* can be expected to be able to diffuse in water via hydrogen (H) exchange, analogous to the proton-exchange reaction in the case of the hydroxide anion (OH^-).[12,13] A detailed investigation has led to a clear understanding of the nature and transport mechanism of OH^- in aqueous solution.[14,15] In the case of OH*, it is believed that this species unselectively 'snatches' an electron from any molecule due to the unpaired electron in its electronic structure. Therefore, a H-hopping chain reaction may be anticipated in aqueous solution; however, such a process has not been previously demonstrated by experimental or computational studies owing to the immense challenges that OH* reactivity and lifetime have posed. Motivated by the apparent lack of data for OH*, the inherent difficulties faced in its experimental detection, and the inconsistency in the rather limited number of molecular dynamic studies[12,13,16,17] on the chemistry of this important chemical species in liquid water, we have performed extensive Car−Parrinello molecular dynamics simulations with a large 63·H_2O−OH* system. In a very recent article[18] we have shown that previous theoretical results[12,13,16] with smaller systems were contaminated by system size effects, being biased by the presence of a three-electron two-centered hemibond structure between the oxygen atoms of a water molecule and the radical. This hemibond is an apparent artifact of the self-interaction error,[19] which is known to effect GGA DFT functionals, and has been demonstrated to decrease significantly as the system size (number of water molecules) is increased in this particular system.[18,20] Here we provide insights into the local hydration structure and mobility of OH* in aqueous solution, demonstrating that the H-transfer between a OH* and a water molecule can be a very rapid reaction and revealing key aspects of this process.

Received: September 20, 2011
Published: November 22, 2011

dx.doi.org/10.1021/ja208874t | J. Am. Chem.Soc. 2012, 134, 532−538

METHODS

The standard Car–Parrinello[21] DFT-based ab initio molecular dynamics method was used with the CPMD[22] code to study 63·H_2O–OH* systems within a 12.56 Å cubic simulation box. Periodic boundary conditions were applied, and the simulation temperature was set to 310 K. The local spin density (LSDA) functional theory was used to account for the unpaired electron on the OH*. The following two different density functionals were utilized and compared: the gradient-corrected exchange-correlation energy functionals of Becke–Lee–Yang–Parr[23,24](BLYP) and the HCTH/120.[25] BLYP was included since it was previously applied in the study of systems of 31 H_2O molecules and a hydroxyl radical.[12,13,16] The HCTH/120[25] functional was also employed because it has been reported to better reproduce the properties of liquid water.[26,27] This particular functional is a highly parametrized GGA functional which was fit to a large set of empirical molecular properties. For our simulations, we have primarily applied the HCTH/120 functional and the Troullier–Martins norm conserving pseudopotential,[28] where the valence electronic wave function is described with a plane wave basis with an energy cutoff of 90 Ry which provides a reasonable basis set convergence for this particular system. In addition, we compare the results obtained from the HCTH/120 functional with those obtained with the BLYP functional with the Goedecker[29] norm-conserving pseudopotential and a valence electronic wave function described with a plane wave basis with a 75 Ry energy cutoff since this scheme was previously applied in the study of systems with 31 H_2O molecules and a hydroxyl radical.[12,13,16] We use this scheme with the BLYP functional for both small (31·H_2O–OH*) and large (63·H_2O–OH*) systems for consistency. Tests with the BLYP functional in combination with either pseudopotentials gave the same results. In general, the parameters used for the dynamics followed those used in previous CPMD simulations for aqueous OH* systems[16] where a fictitious mass of 600 au was utilized in the present study, whereas previous calculations employed 600 au and 800 au.[16] Taking into account the importance of a reasonable selection of the fictitious electronic mass in a Car–Parrinello molecular dynamic simulation, the Supporting Information explores the possible impacts of the selected parameters. The fictitious electron kinetic energy and the dynamics of atoms were controlled by a chain of three Nose–Hoover thermostats[30] operating at characteristic frequencies of 6000 cm^{-1} and 2000 cm^{-1}, respectively. During the 7 ps equilibration and the subsequent 50 ps of simulation, the total energy was monitored as well as the kinetic energy of the fictitious electronic degrees of freedom. The average fictitious kinetic energy was maintained at levels of 0.06 Ha and remained stable during the whole simulation. The time step was set to 0.1 fs.

Constrained MD and Metadynamics. The free energy of the hydrogen transfer reaction between the hydroxyl radical and a water molecule was determined using both constrained molecular dynamics[31] and metadynamics[32] simulations. This is a challenging unitary reaction (OH* + H_2O → H_2O + OH*) to study in liquid water, due to the relatively small barrier for the transfer process and the possible involvement of other neighboring water molecules. In terms of the constrained MD simulations, the difference between the distances O*–H and O–H was, after considerable testing, selected as a constraint (R). Here, a sequential approach was applied, starting the constrained MD simulations from a configuration that is close to the initial state of the reaction, and from there subsequently starting each new constraint run from the end point of the previous simulation. For each 0.1 Å increment, the average constraint force was measured over a 3 ps trajectory. From such simulations the free energy profile was obtained from a straightforward thermodynamic integration over the coordinate R. Lagrangian metadynamics proved useful for the characterization of the free energy barrier for a 31·H_2O–OH* system with the HCTH/120 functional. For this smaller system the H-transfer reaction is not observed to proceed spontaneously, therefore allowing for reasonable performance of the metadynamics approach. Details of this approach have been extensively published.[32,33] The chosen set of collective variables included $CN_O{}^*{}_{-H}$, representing the coordination number of all hydrogen atoms around the radical oxygen (O*) within a radius of 1.2 Å, and the $CN_H{}^*{}_{-H}$, representing the coordination number of all hydrogen atoms around the radical hydrogen (H*) within a radius of 1.7 Å. After extensive testing these were the only parameters found to be successful in achieving a reasonable description of the H-transfer reaction within metadynamics.

RESULTS AND DISCUSSION

"Inactive" State of OH* in Aqueous Solution. Significant contributions to the knowledge of the local solvation structure of the OH* in aqueous solution can be provided through the simulation of a large 63·H_2O–OH* system. From our results, OH* is found to exist in an "inactive" state, OH*$(H_2O)_4$ (Figure 1, IA), in which OH* has three H-bond-donating neighbors and one H-bond-accepting neighbor (radial distribution functions (RDF) and coordination numbers (CN) for this structure are provided in the Supporting Information). This local solvation structure has been reported by Adriaanse et al. after an empirical self-interaction correction (additive correction to the Kohn–Sham total energy) was included in the DFTMD method to suppress the formation of the hemibond, as an apparent artifact of the SIE in DFT.[34] Tuckerman et al.,[14,15] reported an $OH^-(H_2O)_4$ structure for the OH^- "inactive" state where in this case a four-fold planar coordination around the oxygen atom is observed (Figure 1, IIA). The differences between the "inactive" states of both species can be explained by utilizing the electron localization functions (ELF) for isolated OH* and OH^- shown at the top of Figure 1. ELF provides a useful method for the analysis of electron localization in a chemically intuitive way and indicates spatial regions where electron pairs are most likely to be found.[35] We can deduce from these figures that OH^- has the three lone pair electrons in a delocalized ring structure around the oxygen atom[14,15] supporting the hypercoordination of this species in its "inactive" state (Figure 1, IIA), while for OH* a similarly delocalized continuous ring is shown for the ELF for beta spin–orbitals (ELF-β). In addition, a p-like function for the OH* unpaired electron appears in the ELF of alpha spin–orbitals (ELF-α). This then explains the observation that one of the three accepting hydrogen bonds of OH* is stronger than the other two, which corresponds to the interaction with the OH* unpaired electron. In fact, from the electronic features of the "inactive state"(see Figure 2c, IA) it can be seen that at this point the OH* shares positive spin density with the hydrogen of the closest water molecule, indicative of a stronger interaction with this H-bond-donating neighbor. As can be seen in Figure 2d, IA, the highest occupied molecular orbital (HOMO) is located on the OH* in the "inactive state", while the ELF-α and ELF-β have representative features of an isolated OH* and a water molecule at this point.

In the case of OH^-, a proton-transfer reaction was found to be a fast event in aqueous solution, strongly influenced by structural fluctuations. Within our simulations, spontaneous H-transfers were observed on a roughly 30 ps time scale (three events in a total of 100 ps). In its "inactive" state (Figure 1, IA) the radical seems to be already favorably "pre-coordinated" (with respect to its H-bond-donating neighbors) to accept a hydrogen atom from a neighboring water molecule. If this (cf. Figure 1, IA) were the appropriate solvation structure for the H-transfer reactions, then H-transfers in water could proceed essentially uncontrolled, and consequently, a very high mobility of OH* in aqueous solution would be observed.

H-Transfer Mechanism of Hydrated OH*. There are apparent structural and electronic constraints in the "inactive"

dx.doi.org/10.1021/ja208874t | J. Am. Chem.Soc. 2012, 134, 532–538

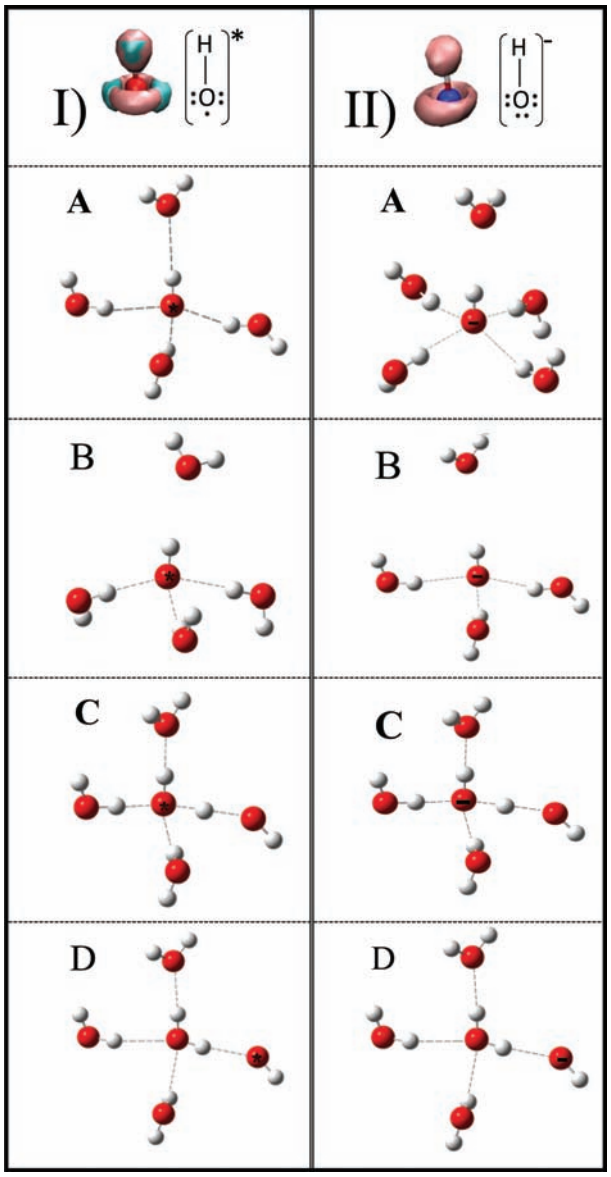

Figure 1. Schematic representation of the first solvation shell of the OH* (column I) and the OH^- (column II)[14,15]for different steps during the hydrogen or proton transfer reaction, respectively, from a nearest neighbor water molecule. (A) Molecular configuration prior to the reaction, corresponding to the "inactive state"; (B) the "active" state; (C) the transition state (TS); and (D) post-transfer.). In these configurations, dotted lines between oxygen and hydrogen atoms indicate $r_{OO} < 3$ Å. ELF isosurfaces (0.85) for isolated OH* and OH^- are shown. For OH*, ELF-β and ELF-α are represented as magenta and cyan isosurfaces, respectively.

state that inhibit the H-transfer reaction. The transformation from the "inactive" $OH^*(H_2O)_4$ (Figure 1, IA) to an "active" $OH^*(H_2O)_3$ arrangement, (Figure 1, IB), occurs through a weakening of the $[H_2O\text{--}HO^*]$ hydrogen bond during local structural fluctuations; the $[H_2O\text{--}HO^*]$ interaction has been already recognized as the most stable for the $OH^*{}_2O$ dimer in the gas phase.[7−11] Here we define the "active state" as the configuration from which the reaction is observed to proceed. Hence, the "active state" state shown in Figure 1, IB is necessarily visited before the H-atom can be transferred. This is potentially the rate-limiting step for the H-transfer reaction. This finding is consistent with the frequency observed for the H-transfer events during our simulations, as the OH* needs to experience the appropriate structural fluctuations to escape from the "inactive"state.

As further evidenced below, in its "pre-transition" state the OH* takes on some aspects of OH^- character. In this state OH* also has a three-fold coordination, as in Figure 1, IB, but the hydrogen atom has started to be transferred, although is still not fully shared by the two oxygens (named IB* in Figure 2). Specifically, a charge polarization of the $(H_3O_2)^*$ complex is observed in this state with the development of a partial negative charge on the hydroxyl moiety. A similar charge polarization was observed by Mitroka et al.[5] when studying the influence of water molecules in the reactivity of the OH* with organic compounds (i.e., hydrogen atom abstraction). This movement of electron density to the OH* moiety is visualized in Figure 2, IB*, which shows the structural and electronic features for the "pre-transition" state. From this figure an early electron movement is evident compared to the position of the hydrogen atom (or proton) (c.f. evolution of the HOMO and the spin density from IA to IB). The chemical potential difference between the α and β states at each identified stage (IA: 3.2, IB*: 0.0, IC: 1.15 and ID: 2.99 (kcal/mol)) is also indicative of this fact. Although this reaction should be defined as a hydrogen-atom transfer (HAT) reaction, because both the electron and the proton come from the same bond,[36] the electronic features presented in Figure 2 are suggestive of a hybrid mechanism[36] apparently involving aspects of HAT and electron−proton transfer (EPT). As has been previously stated,[36] the definitions of HAT and EPT become blurred in some cases due to the extent of electronic coupling and delocalization involved. In the proton exchange mechanism suggested for the hydrated OH^-, a first-solvation-shell H-bond breaking event also occurs, which transforms the $OH^-(H_2O)_4$ structure (Figure 1, IIA) into an approximately tetrahedral $OH^-(H_2O)_3$ structure (Figure 1, IIB).[14,15] Interestingly then the mobility of OH* in aqueous solution has aspects resembling that of hydrated OH^-, that is the "active" states of both species, $OH^*(H_2O)_3$ (Figure 1, IB) and $OH^-(H_2O)_3$ (Figure 1, IIB)[14] appear rather similar. This could be important to the understanding of chemical reactions in water in which OH^- and OH* are both involved, particularly electron-driven processes.[1,37] At the transition state, the hydrogen atom (or proton) is now fully shared by the two OH moieties, corresponding to the formation of a $(H_3O_2)^*$ entity; at this point the environment around each OH moiety becomes similar (the coordination number is 4.0 around both). The $[H_2O\text{--}HO^*]$ distance shortens dramatically at this point (Figure 1, IC), to facilitate the appropriate pre-solvation of the new formed water molecule. In the case of OH^-, a weak H-bond between the OH^- hydrogen and a H-bond-accepting water is also formed in the transition state (Figure1, IIC). After the H-transfer, the new OH* is formed in its "inactive" $OH^*(H_2O)_4$ state (Figure 1, ID), where a similar situation is observed for the OH^-(Figure 1, IID). The consequence of this process is that the radical center has migrated to a new site in the H-bond network. In the post-transfer state (Figures 1, ID and 2, ID) the new OH* carries the major portion of the spin density, similar to the initial state (Figure 2, IA), with only a small amount of positive spin density appearing near the hydrogen of the closest water molecule. In a general analysis of the ELF functions for the reaction (Figure 2, column b), we note that before the H-transfer (Figure 2, IA) the ELF-α has representative features of an isolated OH* and water molecule,

dx.doi.org/10.1021/ja208874t | J. Am. Chem.Soc. 2012, 134, 532−538

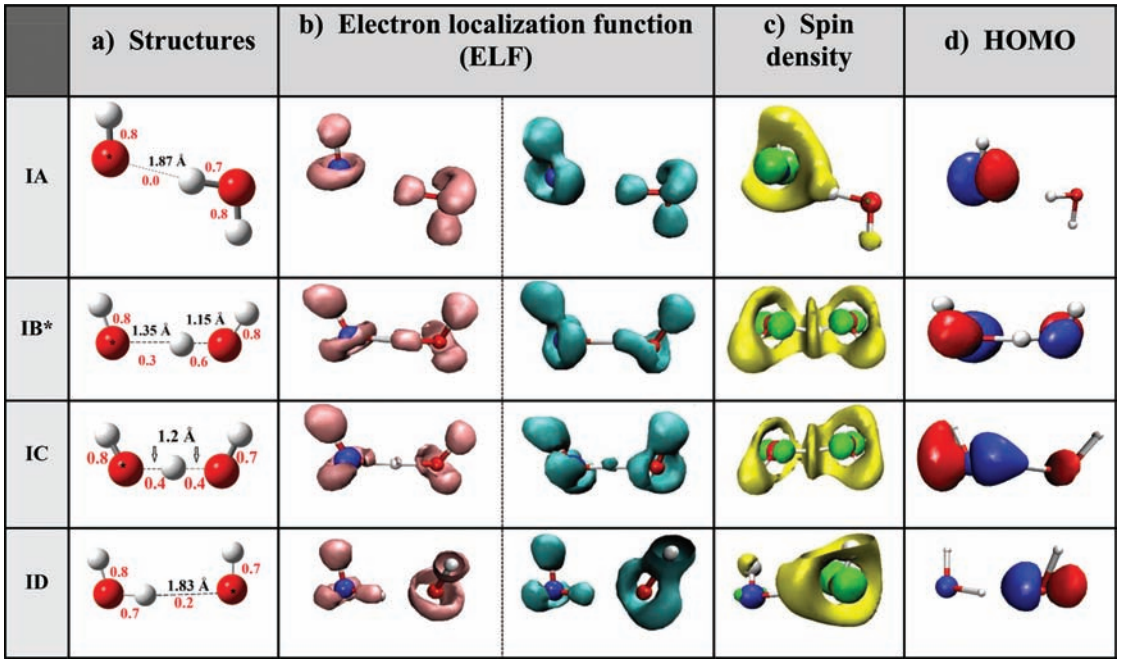

Figure 2. Molecular configurations and electronic features for different states during the spontaneous H-transfer reaction (the OH* and the water molecule involved in the reaction are represented). Row legends: (IA) initial state, (IB*) pre-transition state, (IC) transition state (H_3O_2)* complex, (ID) post-transfer state. A dark-blue sphere represents the oxygen atom of the initial radical. The whole reaction (conversion from IA to ID) occurs in approximately 0.7 ps. Column (a) shows molecular configurations in which the black numbers are atomic distances and red numbers are the bond orders; column (b) presents the ELF-β as magenta isosurfaces (0.85) and the ELF-α as cyan isosurfaces (0.85). Column (c) shows the evolution of the spin density, where the yellow isosurfaces correspond to +0.0004 and green isosurfaces correspond to −0.03. In column (d), the evolution of the HOMO is presented where red and blue isosurfaces have values of −0.03 and +0.04, respectively. For (IA) and (ID) the HOMO is localized on the OH* and is perpendicular to the H-bond with the nearest neighboring water molecule. For (IB*) both HOMO and HOMO−1 orbitals are shown due to the existence of α and β degenerated states centered on the water and OH* oxygens, while at the transition state (IC), the HOMO is shared across the (H_3O_2)* complex.

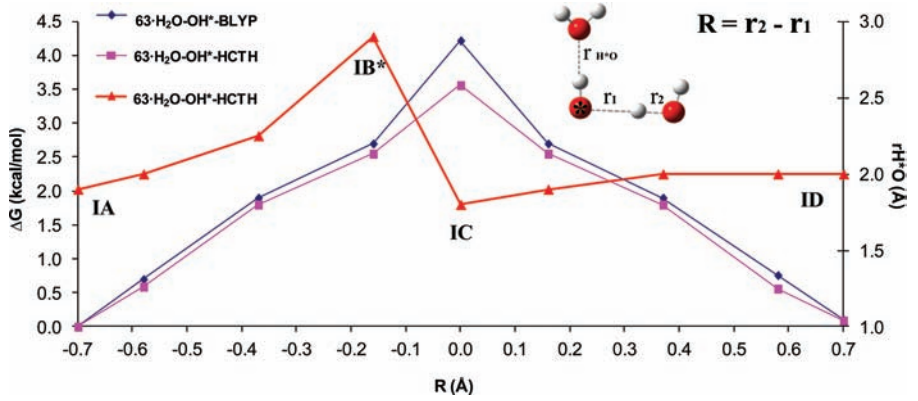

Figure 3. Free energy profiles from constrained molecular dynamics (MD) simulations for the H-transfer reaction between OH* and a neighboring water molecule. The BLYP (blue line) and the HCTH/120 (magenta line) density functionals for the displacement coordinate R (see schematic illustration) were applied. The average r_{H^*O} distance (see schematic illustration) for every constrained MD step is represented by the second axis (right) and the red line.

which become somewhat modified in the pre-transition state (Figure 2, IB*). In the transition state (Figure 2, IC) a symmetric electronic structure, consistent with sharing of electrons, is apparent, with similar character on both oxygen centers. At the completion of the transfer (Figure 2, ID), features typical of the new isolated OH* and water molecule are once again seen. Taking into account the above observations, the diffusion mechanism of OH* in aqueous solution via H-transfer reactions can be summarized as: (1) formation of an "active state" transient $OH^*(H_2O)_3$ structure by the weakening of the $[H_2O$--$HO^*]$ hydrogen bond through local structural fluctuations, (2) formation of a (H_3O_2)* complex with an early electron transfer while the H-atom is still not equally shared between the two oxygens in the "pre-transition" state (EPT), (3) formation of a $[H_2O$--$HO^*]$ hydrogen bond in the transition state to facilitate the appropriate "pre-solvation" of the newly formed water molecule, and (4) completion of the HAT/EPT reaction resulting in a new OH* in the "active state" state and a new water molecule.

Free Energy Barrier for the H-Transfer Reaction. Having established the mechanism, we examine the free energy

dx.doi.org/10.1021/ja208874t | J. Am. Chem.Soc. 2012, 134, 532−538

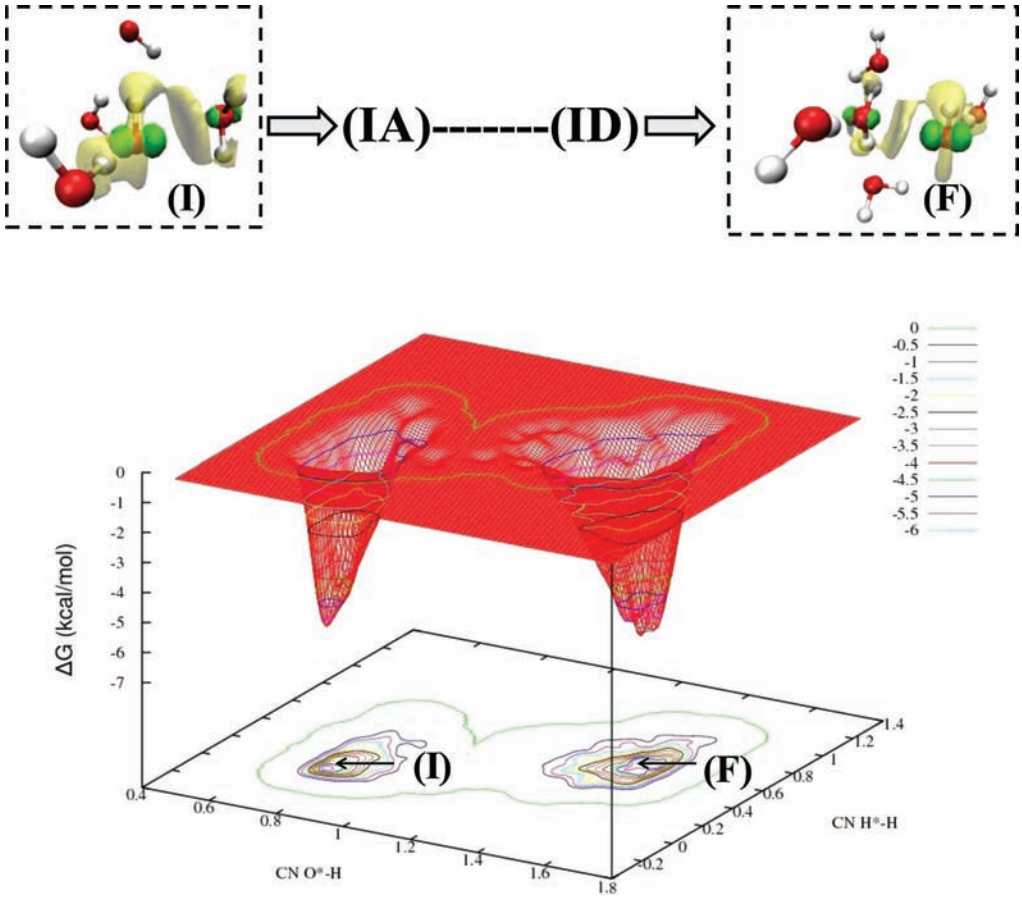

Figure 4. Free energy landscape from a metadynamics simulation for the H-transfer reaction between OH* and a neighboring water molecule for a 31·H_2O−OH* system. The HCTH/120 density functional was applied, the coordination numbers (CN) O*−H (within 1.2 Å) and H*H (within 1.7 Å) are employed as collective variables. Within the initial state of the reaction (labeled I) OH* can be seen sharing positive and negative spin density with the hemibonded water in this small 31·H_2O−OH* system. Applying metadynamics the system evolves to the "inactive" states (IA) shown in Figure 1 and follows the same mechanism from IA to ID (see Figure 1). After the transfer, the new water again forms a hemibond with the newly formed OH* (F).

barrier for this reaction which we conjecture can be a very fast event. From our simulations, a time scale of 30 ps can be considered a rough estimation of the lifetime of the OH* in aqueous solution. Constrained molecular dynamics (MD) simulations[31] were used to estimate the free energy barrier for the reaction (Figure 3). The value obtained of about 4 kcal/mol is in good agreement with experimentally derived values[7] and high level ab initio calculations in the gas phase.[8] In addition, the average $r_H{}^*{}_O$ distance was determined from $g_H{}^*{}_{O(r)}$ for each step of the constrained MD to confirm the crucial influence of this H-bond-accepting neighbor of the OH* during the transfer. As can be observed in Figure 3 (red line), the average $r_H{}^*{}_O$ distances reveal that the interaction with this H-bond-accepting water neighbor weakens significantly just prior to the formation of the transition state, starting at the "active" state for this species and taking a maximum value in the "pre-transition" state (Figure 3, IB, red line). In the transition state (Figure 3, IC, red line) this distance shortens to provide the appropriate coordination in the first solvation shell of the newly formed water molecule. No other significant structural change was observed during the reaction (see Supporting Information).

Metadynamics[32] was also explored as a means to estimate the free energy barrier for this reaction (see details in Methods section). This is a powerful tool that can be used for both reconstructing the free energy and for accelerating rare events at the classical or quantum level.[32] Its application to a 63·H_2O−OH* system proved problematic probably due to the fact that the H-transfer reaction is not a rare event for this larger system (due to the small barrier of this unitary reaction). As we have shown very recently,[18] there is a system size effect in the Car−Parrinello simulations of the OH* in aqueous solution in which, for small 31·H_2O−OH* systems, the OH* oxygen interacts strongly with the oxygen of a neighboring water molecule to achieve a separation of ∼2.4 Å. The unpaired OH* electron is tied down in this three-electron two-centered hemibonded structure, as shown in the spin density of the structure denoted by (I) in Figure 4. Consequently, the H-transfer reaction becomes a rare event in this small 31·H_2O−OH* system. The application of metadynamics did force the system to overcome the hemibonded arrangement before following the same H-transfer mechanism explained above. As illustrated in Figure 4 the initial state (I) corresponds to a local OH* structure (two H-bond-donating neighbors, a H-bond-accepting neighbor and a fourth water molecule forming a hemibond) that was found to be stable for at least 160 ps.[18] The inclusion of repulsive potentials within metadynamics forces the local solvation structure of OH* to evolve to the "inactive" state (IA) previously presented in Figure 1, IA. The process then follows the same mechanism (see Figure 1) in

dx.doi.org/10.1021/ja208874t | J. Am. Chem.Soc. 2012, 134, 532−538

which the "active" state (IB), pre-transition state, transition state (IC), and again "inactive" state (ID) are visited, ending with a H-transfer reaction. As expected for this small system, after the formation of the new radical, the newly formed water quickly rotates to form a new hemibonded structure (structure denoted by (F) in Figure 4). Interestingly, this artificial dynamics yields a free energy barrier that is only somewhat (1−2 kcal/mol) higher than the constrained MD result for the reaction profile given in Figure 4, which is consistent with the observation that the hemibonded dimer in the gas phase is around 1.8 kcal/mol more stable (with BLYP) than the hydrogen bonded configuration (see the Supporting Information of ref 34). This alternate means confirms that the barrier for this reaction has an upper bound of 6 kcal/mol and is indeed small. A rough estimate for the total activation energy for the proton exchange reaction for OH^- is 3 kcal/mol,[14] and indicates that OH* should be less mobile than OH^- in aqueous solution. This is confirmed by the fact that the self-diffusion coefficient of OH* in water has been estimated as 2.8×10^{-5} cm^2/s[37] (slightly higher than that of water molecules, 2.5×10^{-5} cm^2/s) which is significantly slower than the diffusion coefficient of OH^- in aqueous solution (5×10^{-5} cm^2/s).[16] A rough estimate from the present work of the self-diffusion coefficient of OH* in aqueous solution is similar to that of a water molecule (see Supporting Information). Interestingly, this value of the diffusion coefficient is comparable to previous estimates from experiment.[38] The H-transfer reaction can therefore represent an alternative means of diffusion of the radical under appropriate conditions and could contribute significantly to the mobility of OH* in solution.

CONCLUDING REMARKS

Overall, the H-transfer reaction appears to exhibit a hybrid mechanism involving aspects of both HAT and EPT, with a slight polarization of the pre-transition $(H_3O_2)^*$ complex. Our simulation results strongly support a very recent spectroscopic observation[37] made during the irradiation of OH^- in aqueous solution, in which a novel geminate recombination channel of the electron and OH* was claimed to arise from ultrafast H-transfers from neighboring water molecules. While the direct detection of the explicit transfer would be very challenging, in part because of its very short subpicosecond time scale, experimental confirmation can now be undertaken with the use of the microscopic details provided by this work. Our results evidence that H-transfer may represent an alternative mechanism for OH* diffusion in water; this would suggest that OH* mobility via H-transfer reactions can be rather sensitive to the local environment and its fluctuations. Given the great importance of this highly reactive species to a broad spectrum of scientific and industrial fields, detailed studies focused on exploring these mechanisms further is clearly warranted. For example, theoretical investigations probing the possible impact of quantum effects would seem desirable, although would be significantly more challenging than the extensive computations of this work.

ASSOCIATED CONTENT

Supporting Information

Radial distribution functions and coordination numbers; possible effects of the electronic fictitious mass and system size on the local structure; estimation of the self-diffusion coefficient of OH* in aqueous solution; details of metadynamics simulations; full list of authors of reference 1. This material is available free of charge via the Internet at http://pubs.acs.org.

AUTHOR INFORMATION

Corresponding Author

pkusalik@ucalgary.ca

ACKNOWLEDGMENTS

We are grateful for the financial support of the Natural Sciences and Engineering Research Council of Canada and the Canadian Foundation for Innovation. We also acknowledge computational resources made available via WestGrid (www.westgrid.ca) and the University of Calgary. E.C.-H acknowledges Prof. Dr. Alberto Rolo-Naranjo for his help with the processing codes and Dr. Daniel Boese for useful discussions.

REFERENCES

(1) Garrett, B. C.; et al. *Chem. Rev.* **2005**, *105*, 355−390.
(2) Isaksen, I. S. A.; Dalsøren, S. B. *Science* **2011**, *331*, 38−39.
(3) Allodi, M. -A.; Dunn, M.-E.; Livada, J.; Kirschner, K. -N; Shields, G.-C. *J. Phys. Chem. A* **2006**, *110*, 13283−13289.
(4) Manda, G.; Nechifor, M. -T.; Neagu, T.-M. *Curr. Chem. Biol.* **2009**, *3*, 342−366.
(5) Mitroka, S.; Zimmeck, S.; Troya, D.; Tanko, J.-M. *J. Am. Chem. Soc.* **2010**, *132*, 2907−2913.
(6) Vohringer-Martinez, E.; Hansmann, B.; Hernandez-Soto, H.; Francisco, J. S.; Troe, J.; Abel, B. *Science* **2007**, *315*, 497−501.
(7) Dubey, M. K.; Mohrschladt, R.; Donahue, N. M.; Anderson, J. G. *J. Phys. Chem. A* **1997**, *101*, 1494−1500.
(8) Uchimaru, T.; Chandra, A-K; Tsuzuki, S.; Sugie, M.; Sekiya, A. *J. Comput. Chem.* **2003**, *24*, 1538−1548.
(9) Soloveichik, P.; O'Donnell, B.-A; Lester, M.-I. *J. Phys. Chem. A* **2010**, *114*, 1529−1538.
(10) Du, S.; Francisco, J.-S.; Schenter, G.-K.; Iordanov, T.-D.; Garrett, B.-C.; Dupuis, M.; Li, J. *J. Chem. Phys.* **2006**, *124*, 224318−15.
(11) Galano, A.; Narciso-López, M.; Fransisco-Marquez, M. *J. Phys. Chem. A* **2010**, *114*, 5796−5809.
(12) Vassilev, P.; Louwerse, M.-J.; Baerends, E.-J. *Chem. Phys. Lett.* **2004**, *398*, 212−216.
(13) Vassilev, P.; Louwerse, M.-J.; Baerends, E.-J. *J. Phys. Chem. B* **2005**, *109*, 23605−23610.
(14) Tuckerman, M. E.; Marx, D.; Parrinello, M. *Nature* **2002**, *417*, 925−929.
(15) Tuckerman, M. E.; Chandra, A.; Marx, D. *Acc. Chem. Res.* **2006**, *39*, 151−158.
(16) Khalack, J.-M.; Lyubartsev, A.-P. *J. Phys. Chem. A* **2005**, *102*, 378−386.
(17) VandeVondele, J.; Sprik, M. *Phys. Chem. Chem. Phys.* **2005**, *7*, 1363−1367.
(18) Codorniu-Hernández, E.; Kusalik, P. G. *J. Chem. Theory Comput.* **2011**, *7*, 3725−3732.
(19) Lundberg, M.; Siegbahn, P. E. M. *J. Chem. Phys.* **2005**, *122*, 224103.
(20) Hamad, S.; Lago, S.; Mejıas, J. A. *J. Phys. Chem. A* **2002**, *106*, 9104−9113.
(21) Car, R.; Parrinello, M. *Phys. Rev. Lett.* **1985**, *55*, 2471−2474.
(22) CPMD; IBM Corp.: Armonk, NY, 2006; MPI für Festkörperforschung: Stuttgart, Germany, 2001.
(23) Becke, A. *Phys. Rev. A* **1998**, *38*, 3098−3100.
(24) Lee, C.; Yang, W.; Parr, R. *Phys Rev. B* **1998**, *37*, 785−789.
(25) Boese, A. D.; Doltsinis, N. L.; Handy, N. C.; Sprik, M. *J. Chem. Phys.* **2000**, *112*, 1670−1678.
(26) Boese, A. D.; Martin, J. M. *J. Chem. Phys.* **2004**, *121*, 3405−3416.
(27) VandeVondele, J.; Mohamed, F.; Krack, M.; Hutter, J.; Sprik, M.; Parrinello, M. *J. Chem. Phys.* **2005**, *122*, 14515.
(28) Troullier, N.; Martins, J. L. *Phys. Rev. B* **1991**, *43*, 1993−2006.

(29) Goedecker, S.; Teter, M.; Hutter. *J. Phys. Rev. B* **1996**, *54*, 1703−1710.
(30) Martyna, G. J.; Klein, M. L.; Tuckerman, M. *J. Chem. Phys.* **1992**, *97*, 2635.
(31) Sprik, M.; Ciccotti, G. *J. Chem. Phys.* **1998**, *109*, 7737−7745.
(32) Laio, A.; Parrinello, M. *Proc. Natl. Acad. Sci. U.S.A.* **2002**, *20*, 12562−12566.
(33) Ensig, B.; Laio, A.; Parrinello, M.; Klein, M. L. *J. Phys. Chem. B.* **2005**, *109*, 6676−6687.
(34) Adriaanse, C.; Sulpizi, M.; VandeVondele, J.; Sprik, M. *J. Am. Chem. Soc.* **2009**, *131*, 6046−6047.
(35) Becke, A. D.; Edgecombe, K. E. *J. Chem. Phys.* **1990**, *9*, 5397−5403.
(36) Hang, M.; Meyer, T. *Chem. Rev.* **2007**, *107*, 5004−5064.
(37) Iglev, H.; Fisher, M. K.; Gliserin, A.; Laubereau, A. *J. Am. Chem. Soc.* **2011**, *133*, 790−795.
(38) Schwarz, H. A. *J. Phys. Chem.* **1969**, *73*, 1928−1937.